Geotechnical Testing Journal, Vol. 33, No. 1
Paper ID GTJ102375
Available online at: www.astm.org

Hung-Chieh (Jay) Lo,[1] *Kazunori Tabe,*[2] *Magued Iskander,*[3] *and Sung-Ho Yoon*[4]

A Transparent Water-Based Polymer for Simulating Multiphase Flow

ABSTRACT: This study proposes a new water-based transparent material called *Aquabeads* for modeling flow in natural soils. Three types of this material were used to model miscible and multiphase flow transport process in layered soil systems. An optical system was set up to trace flow movements in a two-dimensional (2D) physical model of a soil profile, analyzed using digital image processing to define images of 2D concentration profiles in the model. Model surfactant flushing tests were conducted using a layered soil system and two contaminants, mineral oil and motor oil, in order to illustrate the feasibility of using this water-based polymer to visualize geoenvironmental contamination problems. A surfactant solution made of Triton X-100 mixed with sec-butanol alcohol and xanthan gum was used to achieve a recovery ratio of 88.5 % of motor oil and 95.8 % of mineral oil. Because a transparent soil is used, the optical systems allows for visualizing surfactant flushing. Addition of xanthan gum to increase viscosity prevents mineral oil's downward migration, thus significantly enhancing the oil recovery. The increase in viscosity of the surfactant prevents motor oil from bypassing the plume, thus enhancing recovery by up to 20 times. The study demonstrates that Aquabeads are suitable for modeling multiphase flow, particularly in educational settings.

KEYWORDS: model, multiphase flow, tank test, NAPL, silica gel, silica powder, transparent soil, glass beads, digital image processing, educational, geoenvironmental, groundwater, surfactant flushing, Aquabeads

Introduction

Soil contamination by non-aqueous phase liquids (NAPLs) has been a significant environmental concern for many decades. Many laboratory studies have established that surfactant flushing greatly aids in remediation of contaminated soils (Chevalier and Petersen 1999; Mulligan et al. 2001). Nevertheless there are still some obstacles to be addressed. For example, Robert et al. (2006) described many factors including soil heterogeneity, location of organic phase, mobility ratio, flow rate, and flow path that may seriously reduce the flushing efficiency. Besides, when inappropriate surfactants are used, undesirable liquid crystals and gels may form, causing problems such as pore plugging and reduction of permeability (Dwarakanath et al. 1999; Yoon 2006). Additionally, Pankow and Cherry (1996) reported that the liquid formed after contaminants were solubilized by the surfactant solution, which may be denser than groundwater, thus migrating downward before being captured by the extraction well.

Employing visualization techniques to explore the aforementioned obstacles is very helpful in understanding the performance of surfactant flushing. The conventional approaches, such as laboratory two-dimensional (2D) experiment using glass tanks packed with soils, have been conducted by some researchers. For example, Conrad et al. (2002) built heterogeneous sand models to visualize the mechanism of trichloroethane (TCE) recovery during flushing different surfactant solutions. Photographs and digital image analysis were used to illustrate the interactions between the TCE and the surfactant solutions. Several goals have been obtained by these experiments: (1) To trace the movement of the TCE during the flushing, (2) to evaluate the efficiency of different surfactant solutions, and (3) to observe how heterogeneous conditions affect the test. Kostarelos et al. (1998) employed a similar test to establish that downward migration of the solubilized TCE is preventable if a suitable surfactant solution is used. Similarly, Chevalier et al. (1998) performed a test to visualize the ability of a surfactant in recovering gasoline contaminated soils. The pictures showed that the position and thickness of the gasoline lens were obviously changed after surfactant flooding. These studies establish that 2D tank tests offer a good approach to visualize surfactant flushing. However, tank tests employing natural soils allow for visualizing the process at the boundary of the glass tank only. Transparent soils can potentially allow for spatial measurements of three-dimensional (3D) multiphase flow in heterogeneous media particularly if a laser excited fluorescent dye is used (Aeby 1998; Huang et al. 2002).

This paper presents the flow properties of Aquabeads, a transparent material that can be utilized in model studies to investigate pollutant transport problems. In addition, the paper presents the results of a demonstration of surfactant flushing in a model of this material.

Background

In recent years, several experimental flow studies have been performed using transparent synthetic soils made of amorphous silica gels and powders (Mannheimer and Oswald, 1993; Welker et al. 1999; Liu et al. 2005). Glass beads have also been widely used in research of 2D flow problems (Corapcioglu et al. 1997; Huang et al. 2002; Lunati et al. 2003; Theodoropoulou et al. 2003; Gaganis et al. 2005). Fluoride salts such as cryolite have also been successfully used for color image analysis of contaminants and bacterial growth

Manuscript received February 19, 2009; accepted for publication September 25, 2009; published online December 2009.

[1]Engineer, Geotechnical Engineering Research Center, Sinotech Engineering Consultants, Taipei 110, Taiwan.

[2]Ph.D., Post Doctoral Research Fellow, Polytechnic Institute of New York Univ., New York, NY 11201.

[3]Ph.D., P.E., Associate Professor, Polytechnic Institute of New York Univ., Six Metrotech Center, Brooklyn, New York, NY 11201 (Corresponding author), e-mail: iskander@poly.edu

[4]Ph.D., Post Doctoral Research Fellow, Polytechnic Institute of New York Univ., New York, NY 11201.

FIG. 1—*No smoking sign viewed through 2.8 cm thick Aquabeads 200 in a Plexiglas mold with internal dimensions = 40 × 2.8 × 14.7 cm³.*

in porous media (Rashidi et al. 1997). Image analysis has been successfully applied for the transformation of dye intensity distribution in transparent soils to the solute concentration profile, which enables the exploration of hydrodynamic dispersion phenomena of pollutants transport (Iskander et al. 2010). Although these materials possess potential advantages in modeling many flow situations, they still have some limitations. For example, the pore sizes, porosities, and permeability of glass beads are not representative of natural porous media and engender difficulties in simulating flow transport process. Large scaled models using glass beads and amorphous silica powders are also limited by their poor transparency. In addition, in order to achieve transparency using these materials, the refractive index of the solids and pore fluids must be matched using synthetic pore fluids such as mixtures of mineral oil and paraffinic solvents or calcium bromide brine. These pore fluids are difficult to handle and often present difficulties in long term tests due to change in their optical properties with time. Additionally, the degradation of transparency can be a problem in large amorphous silica or glass models.

Properties of Aquabeads

Developing a new water-based transparent soil is desirable to overcome the limitations of available transparent surrogates. *Aquabeads*, a strong water adsorption polymer, was used as the transparent soils in this research. It has the same refractive index like water (1.333) and is produced by Kuraray Chemical Co. in Osaka, Japan. The material is composed of isobutylene and maleic anhydride copolymer, having a density of 980 g/L, water content of 7 % or less, and a *p*H of 9–10.

Although the dry appearance of this material is yellowish, it becomes transparent after absorbing water (Fig. 1). The polymer has a strong affinity to water; it absorbs up to 200 times its own weight in water. Water absorption is stable under different temperature conditions (Table 1). The hydrated *p*H is 8.5–9.5. The material does not

TABLE 1—*Durability of Aquabeads (Kuraray America, Inc. 1998).*

Test Condition	Test Period	Change of Absorbency (mL/g)
Cool water	899 days	194 → 199
70 °C hot water	30 days	193 → 207
100 °C hot water	3 days	200 → 218
30 % NaOH at 80 °C	10 days	14 → 14
Heating 140 °C	24 h	200 → 190
Heating 180 °C	24 h	200 → 180

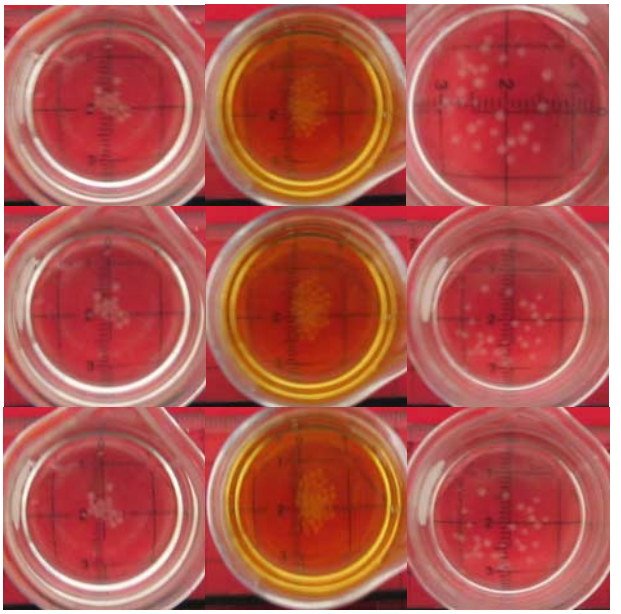

FIG. 2—*NC100 immersed in organic liquids (left: Mineral oil; middle: Motor oil; right: Paraffinic solvent; top: After 1 min; middle: After 1 day; bottom: After 7days).*

absorb organic liquids such as mineral oil, motor oil, and paraffinic solvents even when exposed to them for 7 days (Fig. 2). Research using two types of Aquabeads (Table 2) is reported in this paper as follows:

- *Aquabeads M* is supplied as granular particles resembling fine sand, which becomes an oval spheroid, approximately 4–8 mm in size, after hydration (Fig. 3). Hydration is simply performed by immersing the supplied particles in de-aired water for approximately 4 h. The hydrated particles were sometimes crushed in order to reduce their particle size. The crushed particles were oven dried at 100 °C for 24 h, and the resulting bluish material was re-hydrated with de-aired water. This was done to produce a material with a lower per-

TABLE 2—*Aquabeads used in this study.*

Designation	Type	% Aquabeads in Mixture by Weight (%)	Crushing
NC100	M	0.5	No
C50	M	1	Yes
C75	M	0.66	Yes
200–0.5 %	200	0.5	No
200–1 %	200	1	No

FIG. 3—*Types of Aquabeads: (a) Original specimens and (b) water hydrated specimens (from left to right: C50, 200–1 %, and NC100).*

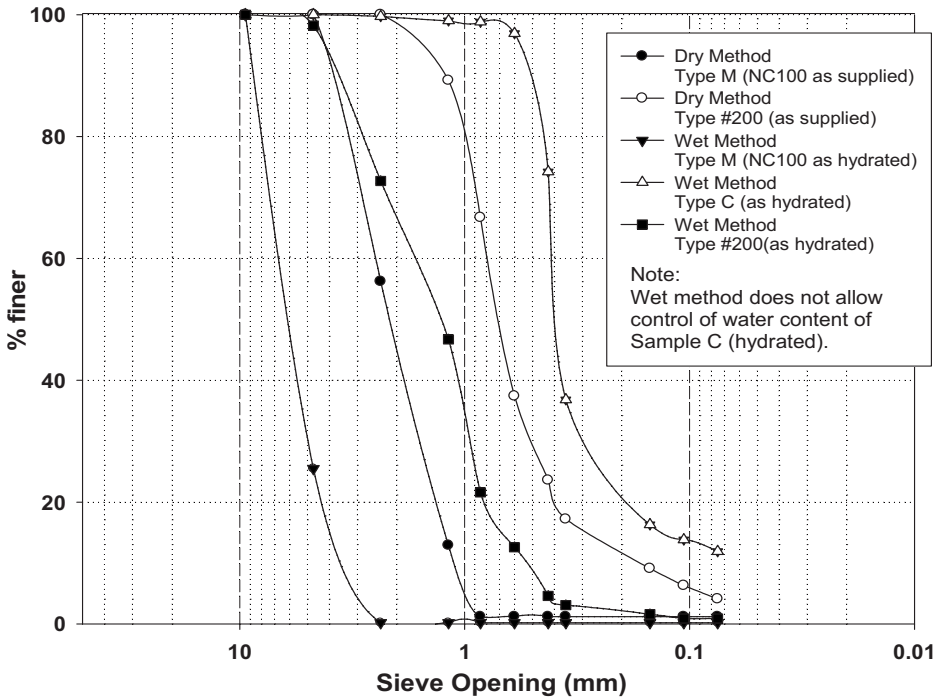

FIG. 4—*Grain size distribution of hydrated Aquabeads.*

meability. The uncrushed material is referred to as *NC100*. Two types of crushed materials are also studied, *C50* and *C75* (Table 2). The crushed materials require a duration of up to 2 days in order to become fully hydrated, de-aired, saturated, and clear. It is believed that crushing only affects the permeability of Aquabeads.

- *Aquabeads No. 200* is supplied as a fine powder that becomes a transparent gel when mixed with water. The percentage of this material (by weight) in the mixture is indicated as either 200–0.5 % (1 g of No. 200 are mixed with 200 g of water) or 200–1 % (2 g of No. 200 are mixed with 200 g of water) in Table 2.

Grain Size Distribution of Aquabeads

Sieve analysis of dry and hydrated Aquabeads is shown in Fig. 4. Tests were performed using the dry method for as delivered material and the wet method for hydrated material. Both dry and hydrated materials exhibit uniform grain size distributions.

Hydraulic Conductivity of Aquabeads

Fixed wall permeability tests were performed with a hydraulic gradient ranging from 3.78 to 5.68 for constant head tests and from 1.52 to 2.27 for falling head tests. Results indicate that the hydraulic conductivity ranges from 7.34×10^{-2} to 2.44×10^{-5} cm/s (Table 3). Flexible wall hydraulic conductivity tests were also performed to study the variation of hydraulic conductivity of the material after being consolidated at different confining pressures (Fig. 5). The material is a water-based soft polymer and thus undergoes volume change due to small variations in confining pressure. For example, when a 20 kPa (2.9 psi) confining pressure was applied, specimens of this material experienced a volume reduction of 6.9 % for NC100, 8.6 % for C50, and 10.5 % for No. 200–0.5 %. Once the volume is decreased, the hydraulic conductivity is reduced. Aquabeads has very weak strength, so hydraulic conductivity may vary with depth, which may be advantageous in modeling natural soil profiles of materials with decreasing permeability with depth in a centrifuge. In any case, further studies of the compressibility and consolidation properties of this material are important to research in future studies.

The modeling conditions in this study are similar to the fixed wall test. In comparison to the hydraulic conductivity of natural soils (Table 4), the material reported in this study is suitable for representing the macroscopic hydraulic conductivities of sands and silts. Finer materials that may be suitable for representing clays are also available, but they were difficult to de-air and make transparent in our initial research.

Experimental Program

Three types of Aquabeads were used for modeling soils with different relative hydraulic conductivities: (1) NC100 (K=2.8–7.3 $\times10^{-2}$ cm/s) and (2) No. 200–0.5 % (K=4.2–5.6$\times10^{-4}$ cm/s) were used to model permeable porous media and (3) C50 (K

TABLE 3—*Summary of fixed wall hydraulic conductivity tests.*

Type of Aquabeads	Hydraulic Conductivity (cm/s)		Suitable for Representing
	Constant Head Test	Falling Head Test	
NC100	2.81×10^{-2}	7.34×10^{-2}	Sand
C50	1.02×10^{-5}	2.44×10^{-5}	Silt
C75	1.45×10^{-4}	1.85×10^{-4}	Silt
Number 200–0.5 %	5.61×10^{-4}	4.18×10^{-4}	Silt
Number 200–1 %	2.68×10^{-4}	2.54×10^{-4}	Silt

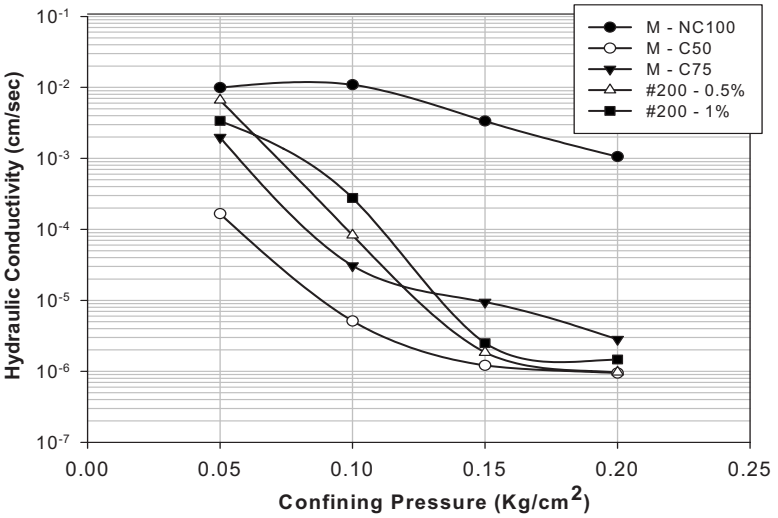

FIG. 5—*Results of flexible wall hydraulic conductivity test.*

$=1-2.4\times10^{-5}$ cm/s) was used to model the less permeable media.

Dyes have been used with success as tracers for ground water flow studies (Flury and Wai 2003). A dyed fluid made of de-aired water and red food coloring was used to conduct miscible flow tests. The red food coloring (Amazon.com ASIN: B00085FA84) is a fine red powder, which easily dissolved in water. This dye was selected since its dye properties were established by Kostarelos (1998) and used with success as a tracer despite having a slightly higher density than water. Additionally, because of the transparency of the surrogate soil, we are able to visualize that (1) the chosen dye is not sorbed to the soil and (2) it possess a stable color spectrum as it travels in the model. In addition, two kinds of oil, white mineral oil (CAS No. 8042-47-5), and motor oil (Castrol 10w40), were dyed using *Oil Red O (*CAS No. 1320-06-5*)* and utilized as contaminants in this study. Because oil does not dissolve in water, multiphase flow transport process could be observed.

Concentration Calibration

The purpose of concentration calibration of dyed fluid is to show that there is a linear relationship between concentration and fluorescence, which in turn is proportional to image intensity. A *Spectronic 20 Genesys* fluorometer and many 4.5 mL four-sided clear methacrylate cuvettes were used for calibration according to ASTM Standard D5613. The frequency of the light source inside the fluorometer was a 581 nm. Different concentrations of dyed fluids were put into the fluorometer, and their relative emitted fluorescence was measured. Higher dyed concentration corresponds to higher fluorescence intensity. Therefore, by measuring fluorescence, the fluid concentration could be obtained. The concentration of red food coloring and Oil Red O is linear up to 0.5 and 0.0625 g/L, respectively (Fig. 6). The calibration of dyed motor oil was difficult due to its dark color; therefore a calibration was developed using a surrogate made of mineral oil and 0.25 g/L Red O dye, which was approximately as dark as the motor oil mixture. Dye concentration, dye volume, and other testing criteria for miscible flow tests and multiphase flow tests are shown in Tables 5 and 6, respectively.

TABLE 4—*Range of hydraulic characteristics for various natural soils.*

Types of Soils	Hydraulic Conductivity (cm/s)	Intrinsic Permeability (darcy)	Porosity
Clay	$10^{-9}-10^{-6}$	$10^{-6}-10^{-3}$	0.35–0.65
Silt	$10^{-6}-10^{-4}$	$10^{-3}-10^{-1}$	0.35–0.60
Sand	$10^{-3}-10^{-1}$	$1-10^{2}$	0.25–0.55
Gravel	$10^{-2}-1$	$10-10^{3}$	0.20–0.40

Packing of Aquabeads for Two-Dimensional Flow Test

A Plexiglas tank with internal dimension $40.0\times2.8\times14.7$ cm^3 was used to perform flow tests. Although a 2.8 cm wide model is used in this study, larger models up to 8.0 cm wide that can be used for 3D modeling, were also transparent. In order to generate a uniform horizontal flow through the model, two filters made of stainless steel screens were placed at each end of the model. First, Aquabeads were immersed in de-aired water until the desired water

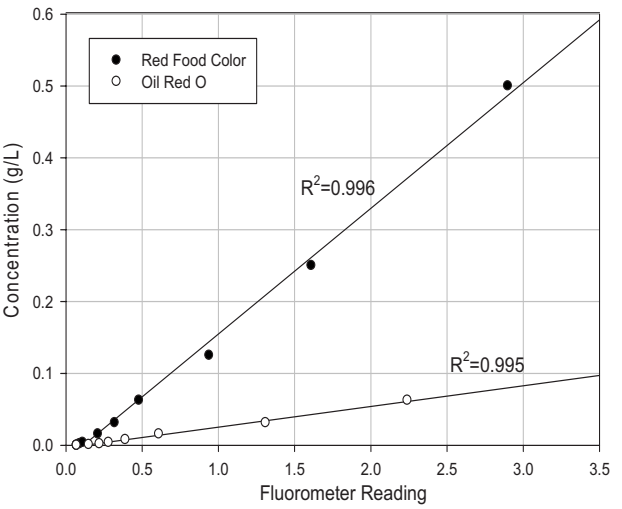

FIG. 6—*Linear range of calibration curve of red food coloring and oil red O.*

TABLE 5—*Criteria of miscible flow tests.*

	Single Layer		Double Layer	
Testing Criteria	100 %, NC-100	100 %, Number 200–0.5 %	75 % NC-100 over 25 % C-50	75 % Number 200–0.5 % over 25 % C-50
Dye concentration (g/L)	0.5	0.5	0.5	0.5
Dye volume (mL)	29.43	30.73	19.64	21.75
Hydraulic gradient	0.038	0.075	0.038	0.038
Flow rate (mL/min)	0.92	0.8	0.98	0.87

absorption was achieved. Next, the hydrated material was poured into the model. During the pouring process, it was necessary to stir the Aquabeads to release air bubbles entrapped in the pore space. Finally, a cover plate with a gasket was screwed tightly onto the model to prevent leakage (Fig. 1). The effective porosity of various tank models was obtained using miscible flow tests. The effective porosity was 0.22 for NC100 and 0.37 for No. 200–0.5 % models.

Flow System Setup and Effluent Collection

All transparent soil models require saturation of the system since the presence of air with a different refractive index is a major source of opacity. After packing, de-aired water, dyed fluid, and surfactant solutions placed in three reservoirs were introduced to the model through a manual switching valve (Fig. 7). A stable pressure panel board was connected to the reservoirs in order to provide a constant head boundary condition. Initially, water was supplied into the model to ensure good transparency and that constant flow rate was achieved. Next, dyed fluid was injected, and the effluent was collected using cuvettes at the other side of the model. The concentration of each effluent sample was measured using the fluorometer and converted to concentration using the calibration shown in Fig. 6. The measured concentrations were used to obtain the volume of NAPL collected. The testing criteria of the flow tests are summarized in Table 5. It is assumed that changes in the size and shape of the materials during flow are negligible because (1) the model has a constant volume and (2) the effective stress is maintained constant.

Optical System Setup

An optical system was used to obtain the images during the test. A *Cohu* 2622 black and white charge coupled device (CCD) camera

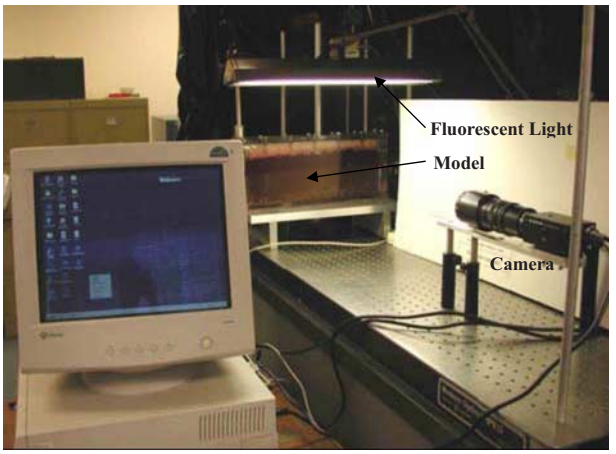

FIG. 8—*Optical system setup.*

with the resolution of 640 × 480 pixels connected to an 8 bit *Matrox* Meteor II frame grabber was set up 1.2 m away from the model, with its optical axis perpendicular to the model (Fig. 8). A fluorescent lamp was placed on top of the model in order to generate a uniform light in the material (Figs. 7 and 8). A black curtain was hung to prevent light scattering. Images were captured during the test and simultaneously imported to the computer.

Image Analysis of Flow Tests

The relationship between image intensity and concentration of a dyed fluid has been described by Corapcioglu and Fedirchuk (1999), Iskander et al. (2010), Niemet and Selker (2001), Ouyang et al. (2002), and O'Carroll and Sleep (2007). Slavik (1994) demonstrated that the relationship can be expressed as

$$F = \phi_f I_0 (1 - e^{-2.303 \varepsilon C l}) \tag{1}$$

where:

F = intensity of fluorescence,
C = concentration of dyed fluid,
I_0 = intensity of the incident light,
l = path length of the light,
ε = molar extinction coefficient of the dye, and
ϕ_f = fluorescence efficiency.

When a low concentration of dyed fluid is used, where $2.303 \varepsilon C l < 0.05$, the relationship can be simplified as

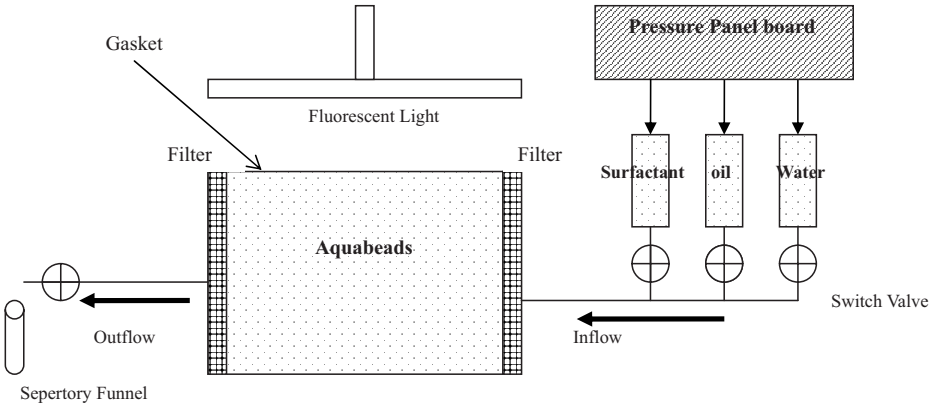

FIG. 7—*Schematic of experimental setup and effluent collection.*

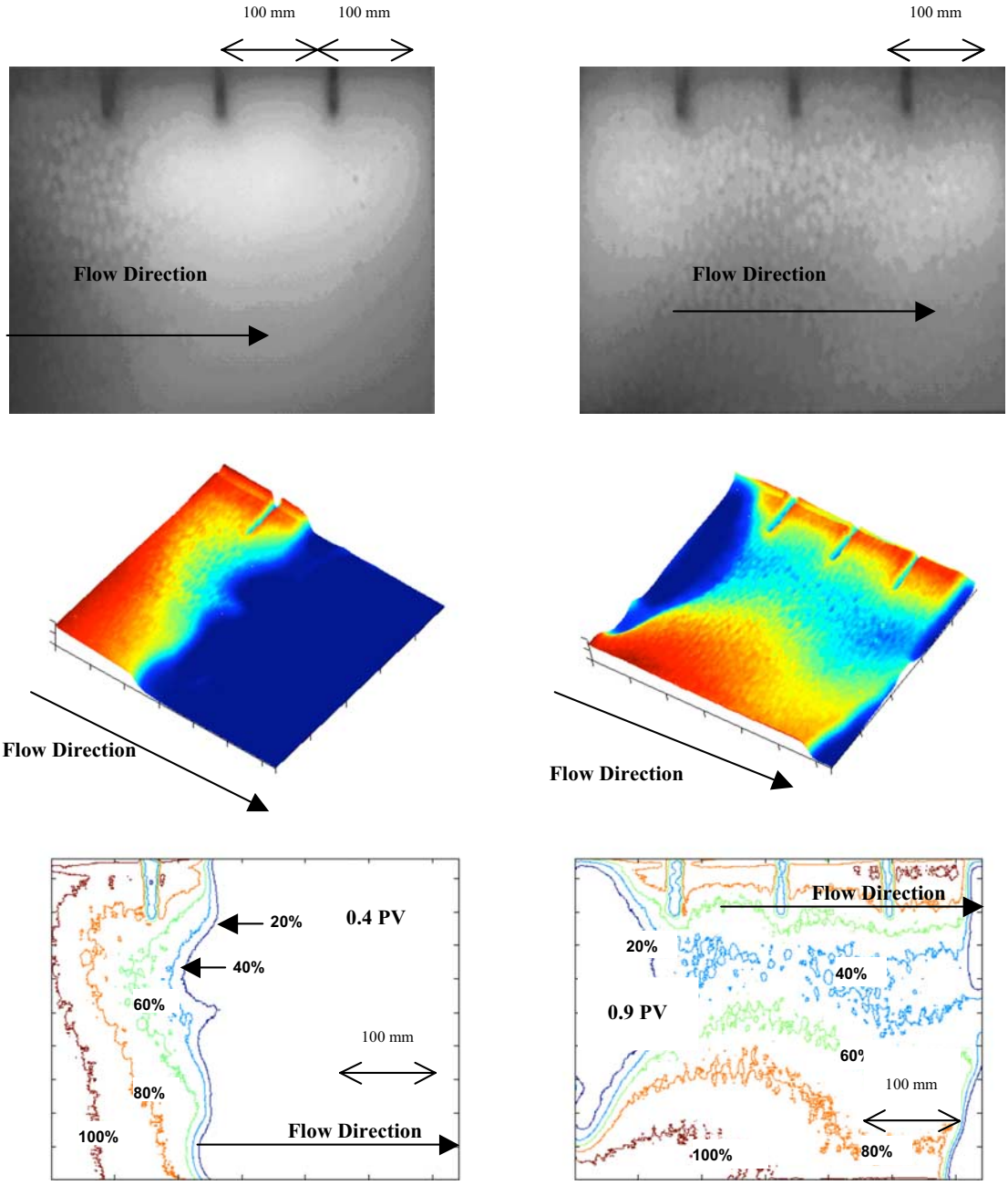

FIG. 9—*Modeling of 2D flow in a single layer of Aquabeads NC100.*

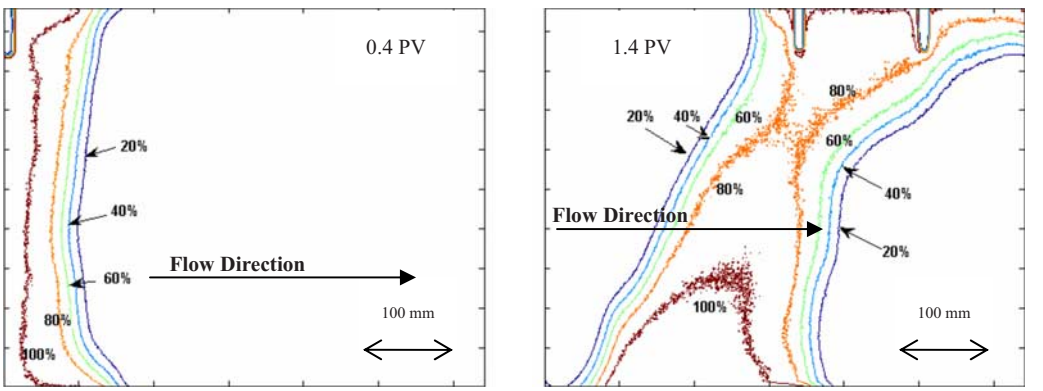

FIG. 10—*Modeling of 2D flow in a single layer of Aquabeads No. 200–0.5 %.*

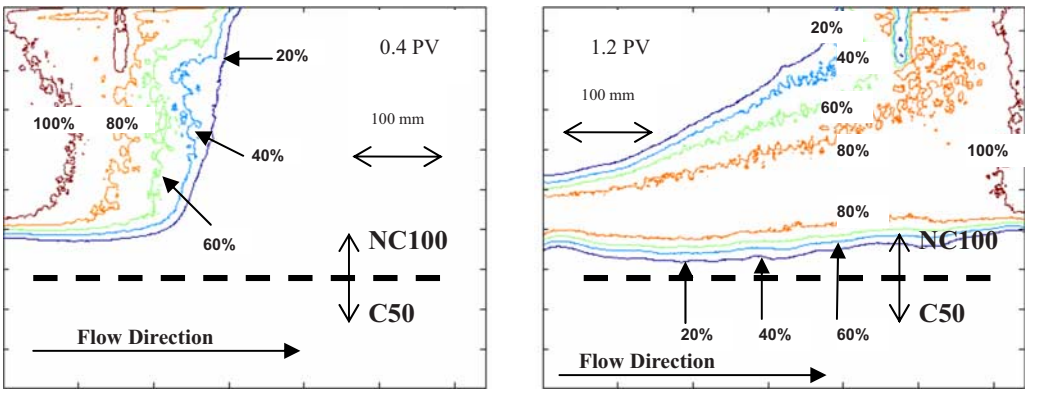

FIG. 11—*Modeling of 2D flow in a double layer of NC100 over C50.*

$$F = 2.303\phi_f I_0 \varepsilon C l \tag{2}$$

So there a linear relationship between concentration and fluorescence. In addition, Aeby (1998) showed that when using a linear detector such as CCD camera, the intensity of fluorescence in the image I is proportional to the fluorescence intensity F, which in turn is proportional to the dye concentration (Fig. 6)

$$I \propto F \propto C \tag{3}$$

The movement of dyed fluid in the middle of the model was captured and imported to a computer during the test. A background correction is required in order to reduce the image noise caused by non uniform lighting and camera response. In this study, the background correction was applied using Adobe Photoshop CS2 filter. The corrected images were imported and analyzed by the image processing toolbox of Matlab®.

Images of Miscible Flow

Movements of the red dye through a single layer of NC100 is shown in Fig. 9 for two time intervals after a 0.1 pore volume (PV) slug was injected using the switching valve and entered the model from the left hand side traveling in a predominantly horizontal direction. The original (side view) images are shown on the top. 3D views of the plume shape are shown in the middle where the intensity value of each point of the plume is projected along the z-axis, which clearly indicates the concentration profile. The 2D intensity contours obtained using Matlab are also shown in the bottom. The contours were scaled to five percentage levels based on the grayscale intensity from the darkest point (100 %) to brightest point (0 %) of the corrected captured image. Both images show clear nature of advection-dispersion process as the dyed fluid migrated thorough the model. Both images indicated that its intensity value was gradually reduced with time.

For a single layer of No. 200–0.5 %, the images indicate that flow lacks uniformity (Fig. 10). Because of its relatively higher hydraulic conductivity and transmissivity, NC100 possess a stronger ability to transmit water compared with No. 200–0.5 %. The plume migration in NC100 is wider than in No. 200–0.5 %. The flow through No. 200–0.5 % was also slower than NC100.

Layered systems of NC100 and No. 200-0.5 over C50 (double layer) are shown in Figs. 11 and 12, respectively. Both models show a "tail of plume" at the interface of the two layers due to the different hydraulic conductivity. "Fingering" was observed in front of flow fringe in the No. 200 model (Fig. 12) due to non uniform packing of the model. A procedure for better model packing in multilayer models is required.

Images of Multiphase Flow

Immiscible flow images (of the middle of the model) after the injection of 0.1 PV (1 PV of NC100=345.3 cm^3) of mineral oil or motor oil are shown in Fig. 13. An upward slower migration is observed due to oil's light density and high viscosity right after its injection into the model. Flushing 20 PV of water did not remove the oil and merely spreads it even when a higher flow rate of water of the order of 2.2–2.5 mL/min was flushed. A mass balance was used to calculate the amount of oil recovered. The recovery after

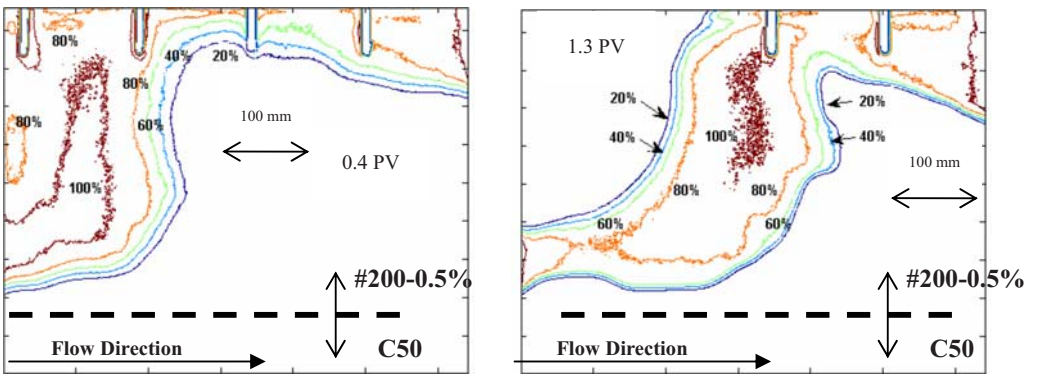

FIG. 12—*Modeling of 2D flow of a double layer of No. 200–0.5 % over C50.*

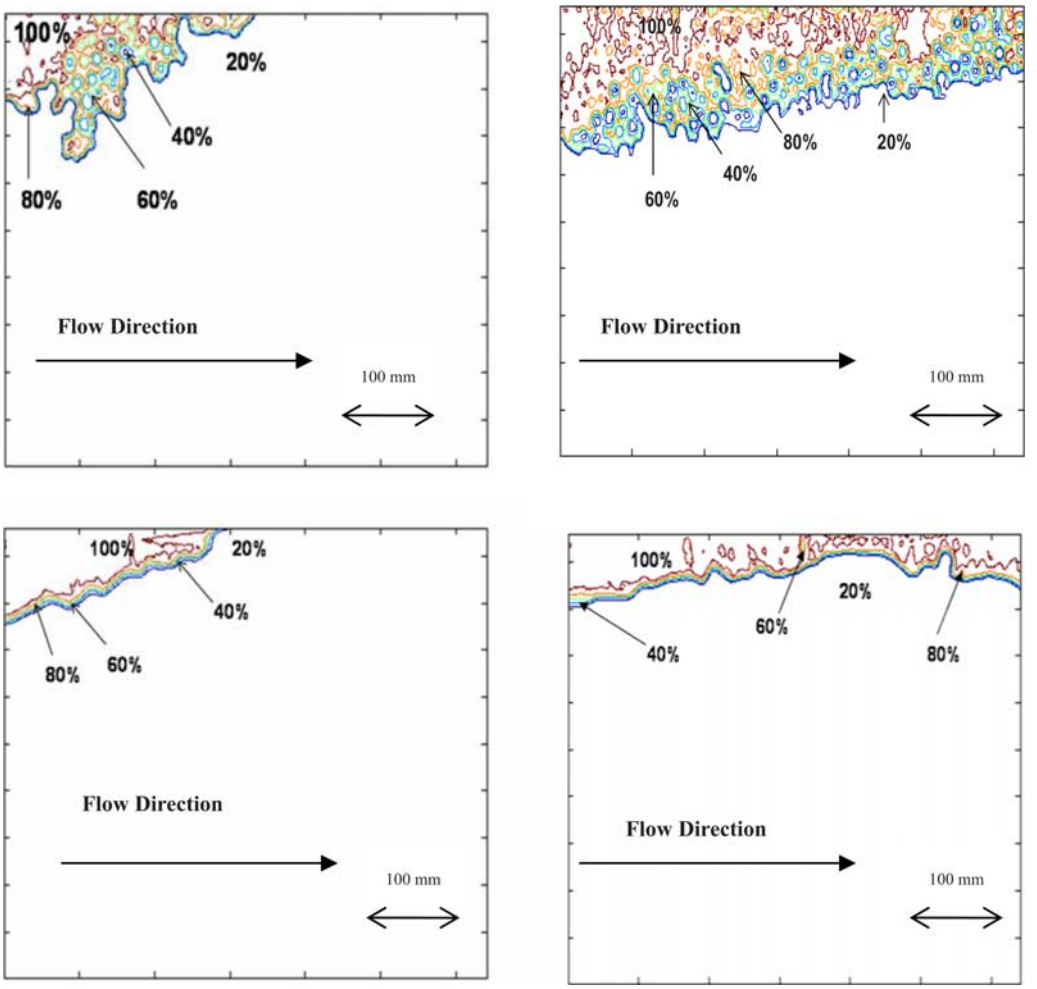

FIG. 13—*Modeling of 2D multiphase flow. Top: Mineral oil (left: After 0.9 PV water flushed; right: After 19.3 PV water flushed). Bottom: Motor oil (left: After 0.4 PV water flushed; right: After 20.3 PV water flushed). Note that flushing with 20 PV of water merely spreads the NAPL.*

flushing 20 PV was less than 5 % of total oil volume injected in the model. It was hard to remove the residual oil from the porous space due to the oil's low water solubility and mobility.

Hydraulic Characteristics of Aquabeads

Hydraulic conductivity measurements were performed during single layer flow tests and was found to be 1.12×10^{-2} and 4.56×10^{-3} cm/s for NC100 and No. 200–0.5 %, respectively. These values are consistent with the conductivities obtained from fixed wall permeability tests. The conductivity of No. 200–0.5 % was one order of magnitude higher than the results of fixed wall hydraulic conductivity test perhaps due to inadequate packing.

The *intrinsic permeability* of NC100 and No. 200–0.5 % was found to be 1.15×10^{-7} cm^2 (11.65 darcy) and 4.67×10^{-8} cm^2 (4.67 darcy), respectively, which are consistent with that of sand.

Transmissivities of NC100 and No. 200–0.5 % are 0.164 and 0.067 cm^2/s, respectively, in the conducted flow tests.

Effective porosity is the pore space of the porous media, which allow the water to pass through. It was estimated by performing a tracer test, where the concentration of the effluent is measured to plot a breakthrough curve. From the breakthrough curve, the swept PV can be computed using the method of first temporal moment, which corresponds to an instantaneous tracer pulse (Himmelblau and Bischoff 1968). When a conservative non-reactive tracer is used, the equations for calculating swept PV and effective porosity, n_e, of one-dimensional flow are

$$\mathrm{PV}=\frac{\sum_{i=1}^{n} C_i V_i \Delta V}{\sum_{i=1}^{n} C_i \Delta V}-\frac{1}{2}V_s \tag{4}$$

$$n_e=\frac{P_v}{V} \tag{5}$$

where:

C_i = concentration of sample,
V_i = cumulative PV,
ΔV = volume of each effluent specimen,
V_s = volume of the injected tracer slug, and
V = bulk volume.

It is believed that Eqs 4 and 5 provide a reasonable approximation of test conditions and can be used. For single layer flow tests, the center of mass of the tracer breakthrough curve (Fig. 14) corresponds to the PV of 345.3 and 569.07 cm^3 for NC100 and No.

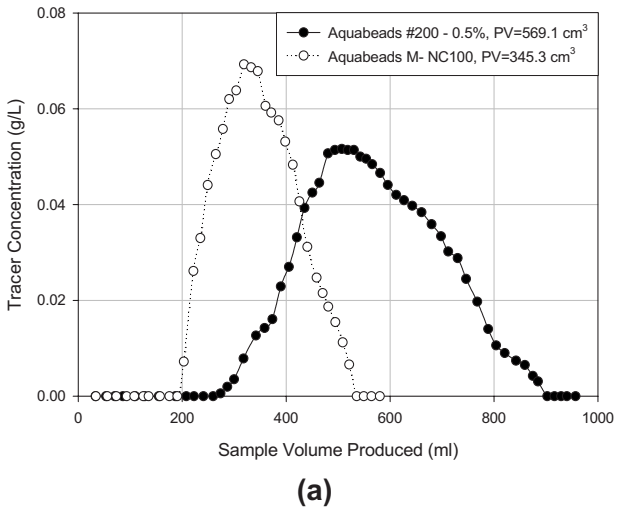

FIG. 14—*Breakthrough curve tracer test: (a) Single layer modeling and (b) double layer modeling.*

200–0.5 %, respectively. For layered (double) system tests, the PV was estimated to be 258.71 cm^3 for NC100 and 450.71 cm^3 for No. 200–0.5 %. The effective porosity of NC100 determined from the double layer modeling was 75 % of the single layer model because the double layer model consisted of 75 % NC100 (top) and 25 % C50 (bottom). In addition, the PV estimated from the double layer modeling of 200–0.5 % was 79 % of the single layer model, a 4 % overestimation. In the double layer tests on No. 200–0.5 %, a small breakthrough curve appeared before the main breakthrough curve due to insufficient sample collection and non uniform model packing. Better result can be expected with better packing and by using an auto-collector with a higher sampling frequency. Fingering observed in the captured images can also be seen from the breakthrough curves shown in Fig. 14(*b*) where falling limbs are much longer and flatter than the rising limbs.

The effective porosities of NC100 and No. 200–0.5 % were found to be 0.22 and 0.37, respectively. The porosity seems rather low for the NC100 compared to typical natural media of this size, probably reflecting the effect of packing flexible particles.

The *hydrodynamic dispersion coefficient* is a mass transport parameter that combines the mechanical dispersion with molecular diffusion. In this research, the accumulated breakthrough curve

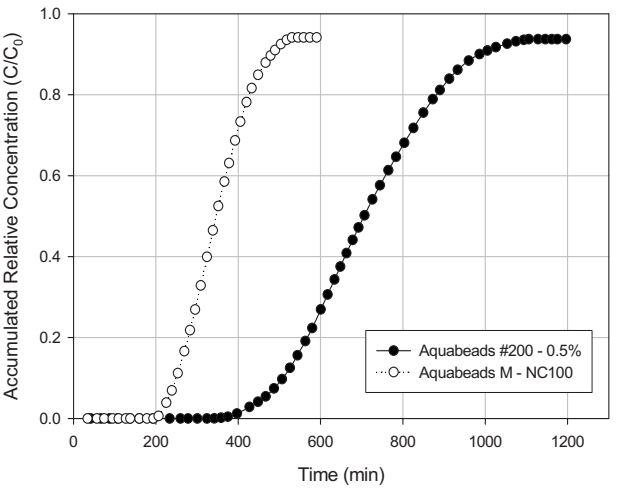

FIG. 15—*Accumulated breakthrough curve of mono layer flow test.*

made from the tracer test is shown in Fig. 15, which resulted in hydrodynamic dispersion coefficient of 3.29×10^{-3} and 1.25×10^{-3} cm^2/s for NC100 and No. 200–0.5 %, respectively.

The *longitudinal dispersion* can be estimated from two points on the breakthrough curve (Fetter 1999). The results show that the longitudinal dispersivity of NC100 is 17.3 mm and that of No. 200–0.5 % is 13.4 mm. This is slightly higher than the expected laboratory range for natural soils, which typically range from 0.1 to 10 mm (Freeze and Cherry 1979). The hydraulic characteristics of Aquabeads NC100 and No. 200–0.5 % are summarized in Table 6.

Modeling of Two-Dimensional Surfactant Flushing

A limited surfactant flushing test was performed to illustrate (1) that Aquabeads can be used to model geoenvironmental contamination problems, (2) the compatibility of the materials and some commonly used surfactants, and (3) the usefulness of visualizing remediation processes.

Phase Behavior Tests

Conducting phase behavior test is essential in order to understand the reactions between contaminants and a given surfactant solution.

FIG. 16—*Phase behavior test after equilibrium. Dark portion of the tube: Dyed mineral oil. Clear portion of the tube: Surfactant solution with different concentrations (from left to right: Triton X-100 with 0.1, 0.05, 0.025, 0.0125, and 0.006 25 % by weight).*

TABLE 6—*Hydraulic characteristics of selected Aquabeads.*

Hydraulic Characteristic	NC100	Number 200–0.5 %
Hydraulic conductivity (cm/s)	1.12×10^{-2}	4.56×10^{-3}
Intrinsic permeability (cm^2)	1.15×10^{-7}	4.67×10^{-8}
Transmissivity (cm^2/s)	0.164	0.067
Porosity[a]	0.22	0.37
Dispersion coefficient[a] (cm^2/s)	3.29×10^{-3}	1.25×10^{-3}
Longitudinal dispersivities[a] (mm)	17.3	13.4

[a]Determined by tracer tests.

Phase behavior provides a basis for surfactant selection and assures the effectiveness of additives (electrolytes, cosolvents, and polymer) and their best surfactant formation. The expected results, such as high contaminant solubilization, fast equilibrium, and minimal liquid crystallization and gel formation, can be observed through these tests (Dwarakanath et al. 1999). Phase behavior tests were performed as follows. First, the surfactant solution and oil contaminants are mixed in a test tube with a 1:1 ratio by volume. Second, the tubes are sealed. Next, the tubes are tumbled ten times to obtain a good mixing of the liquids. Finally, the separation of the liquid phases inside of the tube is observed until equilibrium is reached (Fig. 16), and the time to reach equilibrium is recorded.

Phase behavior tests were performed to select appropriate surfactant solutions, which are compatible with this water-based polymer. All phase tests were performed at 25°C to simulate the temperature during the modeling conditions. Several criteria were used for finding the optimal surfactant solution including (1) fast equilibrium time, (2) flat and mobile oil/aqueous interface, (3) no liquid crystallization or gels forming, and (4) chemical compatibility with Aquabeads. The commercial surfactant *Triton X100* composed of octylphenol ethylene oxide consendate (*CAS No. 9002-93-1*) diluted with deionized water was selected. In addition, in order to eliminate gel/liquid crystals, sec-butanol (*CAS No. 78-92-2*) was used as the cosolvent to mix with X100. Finally, the polymer Xanthan gum was used as an additive to increase the viscosity of the surfactant solution, which improved the performance of the surfactant in layered systems. No liquid crystallization or gels were observed during testing with the selected surfactant solutions shown in Table 7. All phase behavior tests were performed ten times at each selection of concentration of surfactant and cosolvent.

TABLE 7—*Properties of selected surfactant solutions (% by weight).*

	NAPL	Triton X-100	Sec-Butanol	Xanthan Gum
1	Mineral oil	0.025	0.25	0
2	Mineral oil	0.025	0.25	0.03
3	Motor oil	0.025	2.5	0
4	Motor oil	0.025	2.5	0.03

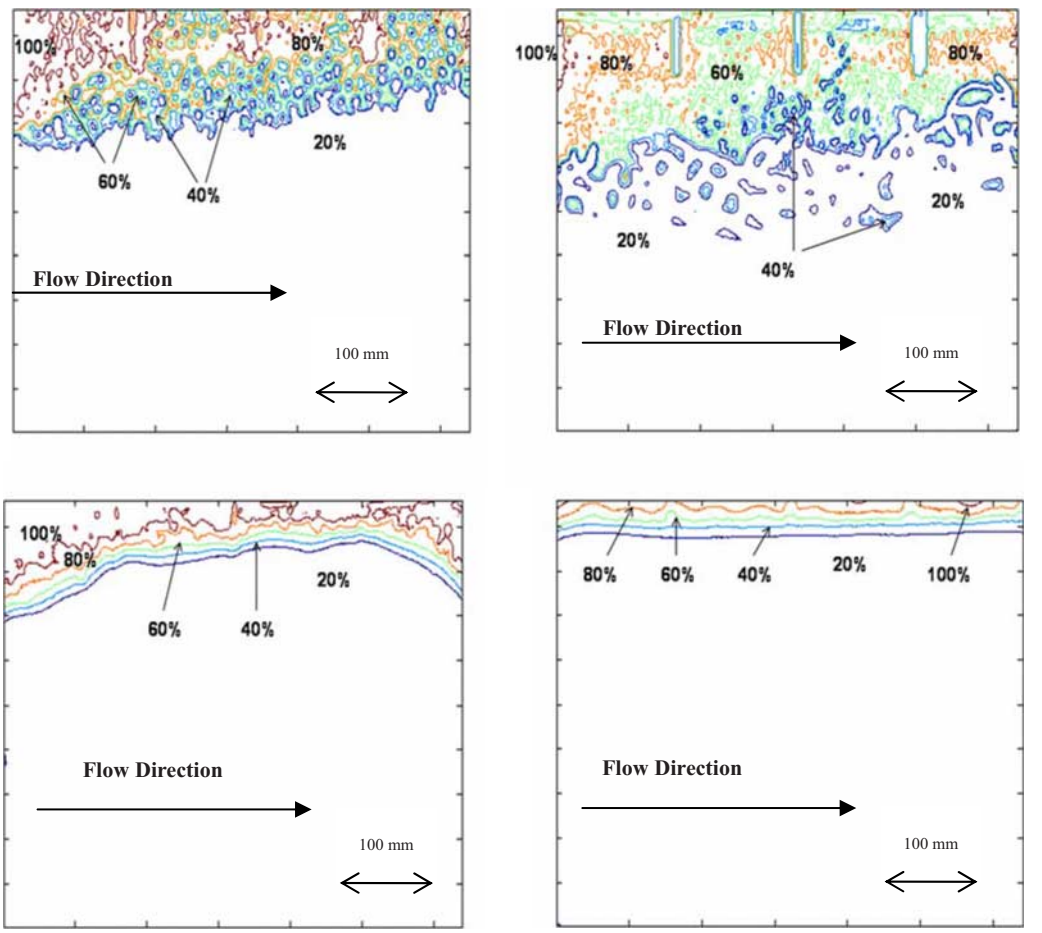

FIG. 17—*2D surfactant flushing. Top: Mineral oil without Xanthan gum (left: Before flushing; right: After 20.9 PV of surfactant flushed). Bottom: Mineral oil with xanthan gum (left: Before flushing; right: After 20 PV surfactant flushed).*

TABLE 8—*Criteria of multiphase flow tests.*

Testing Criteria	Multiphase Flow Modeling	
Oil	Mineral oil	Motor oil
Dyed concentration (g/L)	0.0625	0.25
Volume of dyed fluid (mL)	24.69	25.06
Hydraulic gradient	0.167	0.167
Flow rate (mL/min)	2.21	2.47

Test Setup

A layered model, consisting of 25 % C50 on the bottom and 75 % NC100 on the top, was used. Two kinds of oil, mineral oil and motor oil, were utilized as NAPLS in this study. After the system was set up and a constant flow condition was established, dyed oil was injected into the model, and its residual saturation status was obtained after flushing with a known amount of water. Next, the selected surfactant solution was subsequently injected. The effluent was collected using a glass separatory funnel. Therefore, the amount of water/surfactant solution that had been flushed and the volume of oil that had been recovered were measured. The testing criteria are summarized in Table 8.

Recovery of Mineral Oil

The surfactant solution mobilized the mineral oil trapped in the porous space due to the reduction of interfacial tension. It broke the oil blobs into globules and brought those globules out of the original trapping space. A downward migration of the oil globules was seen during the flushing. It caused the globules to relocate, and finally they were trapped in another porous space. 47.6 % of mineral oil was removed by the surfactant flushing. In contrast, once xanthan gum was added to the surfactant, the oil's downward migration was completely prevented. Xanthan gum significantly increased viscosity, which resulted in a good oil recovery (Fig. 17). A 95.8 % oil recovery was achieved after 20 PVs of surfactant solution were flushed.

Recovery of Motor Oil

Although no downward migration of oil blobs was observed when flushing the surfactant without adding polymer, only 4.4 % of the oil was recovered. Since the motor oil entirely occupied the upper porous space, the surfactant solution traveled primarily through the uncontaminated porous space, thus bypassing the contamination. Therefore, mobilization was reduced due to the limited contact of the surfactant and oil. Inversely, the oil recovery was substantially enhanced when xanthan gum was added. 88.5 % of the oil was recovered after flushing 14.1 PVs of the surfactant solution, which is approximately 20 times the recovery rate achieved without adding polymer (Fig. 18). The recovery rate of both mineral oil and motor oil is shown in Fig. 19.

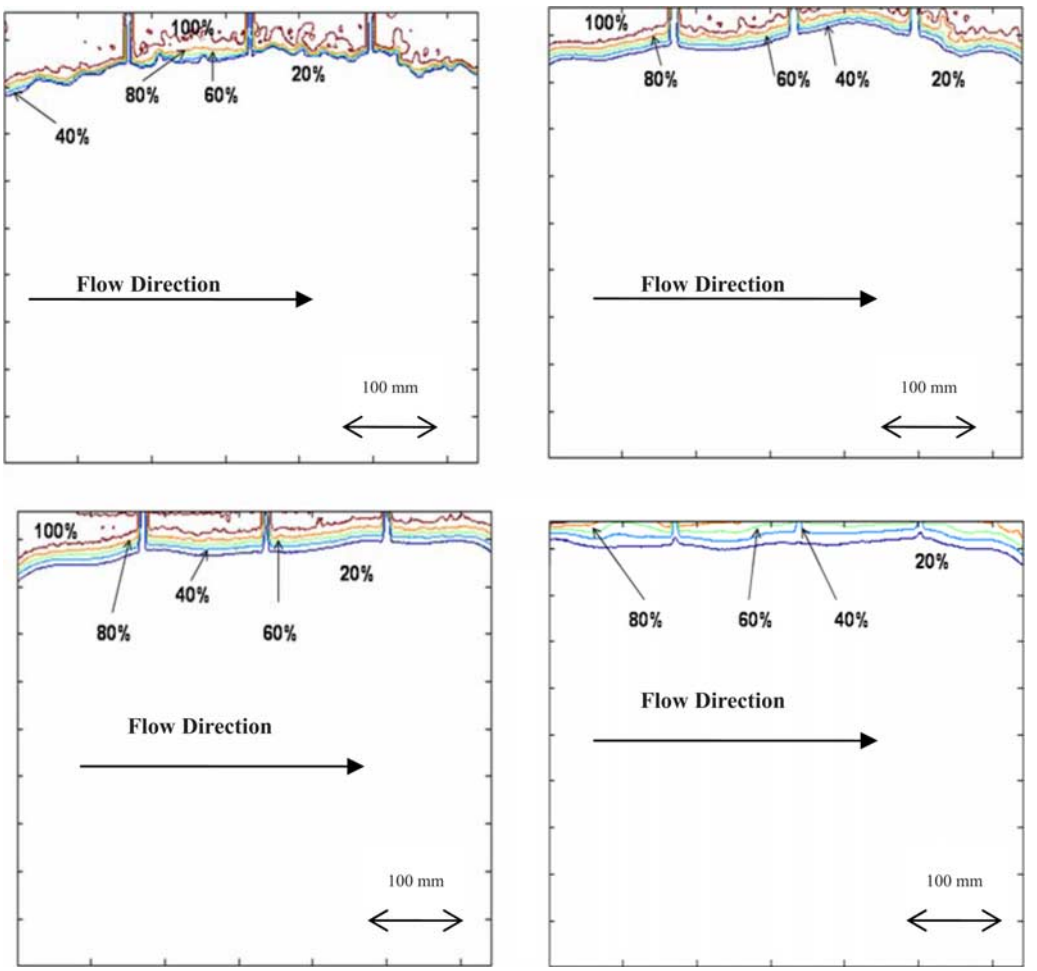

FIG. 18—*2D surfactant flushing. Top: Motor oil without Xanthan gum (left: Before flushing; right: After 11.9 PV surfactant flushed). Bottom: Motor oil with xanthan gum (left: Before flushing; right: After 14.1 PV surfactant flushed).*

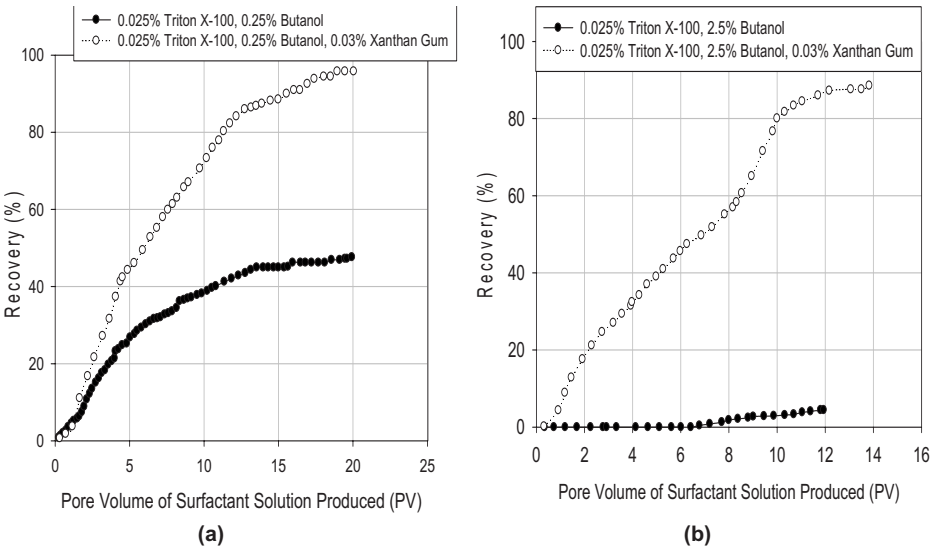

FIG. 19—*Percent recovery: (a) Mineral oil and (b) motor oil.*

Limitations of Aquabeads

Aquabeads are suitable for simulating the macroscopic properties of sands and silts. However the material has the following limitations.

- It cannot be used for unsaturated conditions, in order to maintain transparency.
- Its strength is lower than that of sands and silts, so modeling of coupled processes involving strength and flow is difficult.
- The fluid transport depends in part on contact angle and surface tension, whose values may be quite different for mineral soils and for the Aquabeads. This issue requires further research.

Conclusions and Recommendations

In this study, Aquabeads, a transparent water-based polymer, was used as a surrogate soil. The materials offer a number of advantages over available transparent synthetic soils for modeling flow. First, it is water based. Second, it possesses similar hydraulic characteristics to natural soils. Third, it is compatible with water, oil, selected surfactants, and alcohols used for modeling multiphase flow. Finally, it does not suffer from transparency degradation in large scale models.

Multiphase flow and surfactant flushing tests were simulated using a layered soil system of the water-based material and two contaminants, mineral oil and motor oil. The developed technology allows for visualizing the contamination concentration profiles and the surfactant's sweeping efficiency. This allowed the research team to understand causes of initial poor recovery ratio and develop an appropriate solution. For models contaminated with mineral oil, the addition of xanthan gum reduced the oil's downward migration thus significantly enhancing its recovery. For models contaminated with motor oil, an increase in viscosity of surfactant prevented it from bypassing the plume, thus enhancing recovery by up to 20 times.

This study demonstrates the utility of Aquabeads in evaluating flushing technologies in bench scale model tests prior to conducting in situ surfactant flushing. In the short term Aquabeads are ideal for simulating 2D NAPL transport characteristics, particularly in educational settings including undergraduate laboratories and high schools. In the long term this water-based material may permit 3D modeling of multiphase flow using laser excited fluorescent dyes, thus permitting the study of complex 3D geoenvironmental contamination problems.

References

ASTM D5613–94, 2008, "Standard Test Method for Open-Channel Measurement of Time of Travel Using Dye Tracers," *Annual Book of ASTM Standards*, Vol. 11.02, ASTM International, West Conshohocken, PA.

Aeby, P. G., 1998, "Quantitative Fluorescence Imaging of Tracer Distribution in Soil Profiles," Ph.D. dissertation, Swiss Federal Institute of Technology, Zurich, Switzerland.

Chevalier, L. R. and Petersen, J., 1999, "Literature Review of 2-D Laboratory Experiments in NAPL Flow, Transport, and Remediation," *J. Soil Contaminat*, Vol. 8(1), pp. 149–167.

Chevalier, L. R., Wallace, R. B., and Wiggert, D. C., 1998, "Impact of Surfactant on Configuration of Petroleum Hydrocarbon Lens," *J. Soil Contaminat*, Vol. 7(3), pp. 395–414.

Conrad, S. H., Glass, R. J., and Peplinski, W. J., 2002, "Bench-Scale Visualization of DNAPL Remediation Processes in Analog Heterogeneous Aquifers: Surfactant Floods and In Situ Oxidation Using Permanganate," *J. Contam. Hydrol.*, Vol. 58(1–2), pp. 13–49.

Corapcioglu, M. and Fedirchuk, P., 1999, "Glass Bead Micromodel Study of Solute Transport," *J. Contam. Hydrol.*, Vol. 36(3–4), pp. 209–230.

Corapcioglu, M., Chowdhury, S., and Roosevelt, S., 1997, "Micromodel Visualization and Quantification of Solute Transport in Porous Media," *Water Resour. Res.*, Vol. 33(11), pp. 2547–2558.

Dwarakanath, V., Kostarelos, K., Pope, G. A., Shotts, D. R., and Wade, W. H., 1999, "Anionic Surfactant Remediation of Soil Columns Contaminated by Nonaqueous Phase Liquids," *J. Contam. Hydrol.*, Vol. 38(4), pp. 465–488.

Fetter, C. W., 1999, *Contaminant Hydrogeology*, Prentice-Hall, Englewood Cliffs, NJ.

Flury, M. and Wai, N., 2003, "Dyes as Tracers for Vadose Zone Hydrology," *Rev. Geophys.*, Vol. 41, pp. 2-1–2-37.

Freeze, R. A. and Cherry, J. A., 1979, *Groundwater*, Prentice-Hall, Englewood Cliffs, NJ.

Gaganis, P., Skouras, E. D., Theodoropoulou, M. A., Tsakiroglou, C. D., and Burganos, V. N., 2005, "On the Evaluation of Dispersion Coefficients from Visualization Experiments in Artificial Porous Media," *J. Hydrol.*, Vol. 307(1–4), pp. 79–91.

Himmelblau, D. M. and Bischoff, K. B., 1968, *Process Analysis and Simulation: Deterministic System*, John Wiley & Sons, Inc., New York.

Huang, W. E., Smith, C., Lerner, D., Thornton, S., and Oram, A., 2002, "Physical Modelling of Solute Transport in Porous Media: Evaluation of an Imaging Technique Using UV Excited Fluorescent Dye," *Water Res.*, Vol. 36(7), pp. 1853–1863.

Iskander, M., 2010, *Visualizing Soil Structure Interaction and Multiphase Flow, Nonintrusively*, Springer, New York.

Kostarelos, K., 1998, "A New Concept: Natural Buoyancy for Surfactant Flooding," Ph.D. dissertation, University of Texas at Austin, Austin, TX.

Kostarelos, K., Pope, G. A., Rouse, B. A., and Shook, G. M., 1998, "A New Concept: The Use of Neutrally Buoyant Microemulsions for DNAPL Remediation," *J. Contam. Hydrol.*, Vol. 34(4), pp. 383–397.

Kuraray America, Inc., 1998, "Water Absorbent Resin KI-GEL 201K-F2," Kuraray America, Inc., 200 Park Avenue, New York, NY 10166.

Liu, J., Iskander, M., Tabe, K., and Kostarelos, K., 2005, "Flow Visualization Using Transparent Synthetic Soils," *Proceedings of 16th Int. Conf. Soil Mechanics and Geotechnical Engineering (ICSMGE)*, Millpress, Amsterdam, The Netherlands, Vol. 4, pp. 2411–2414.

Lunati, I., Kinzelbach, W., and Sorensen, I., 2003, "Effect of Pore Volume-Transmissivity Correlation on Transport Phenomena," *J. Contam. Hydrol.*, Vol. 67(1–4), pp. 195–217.

Mannheimer, R. J. and Oswald, C. J., 1993, "Development of Transparent Porous Media with Permeabilities and Porosities Comparable to Soils Aquifers and Petroleum Reservoirs," *Ground Water*, Vol. 31(5), pp. 781–788.

Mulligan, C. N., Yong, R. N., and Gibbs, B. F., 2001, "Surfactant-Enhanced Remediation of Contaminated Soil: A Review," *Eng. Geol. (Amsterdam)*, Vol. 60(1–4), pp. 371–380.

Niemet, M. R. and Selker, J. S., 2001, "A New Method for Quantification of Liquid Saturation in 2-D Translucent Porous Media Systems Using Light Transmission," *Adv. Water Resour.*, Vol. 24, pp. 651–666.

O'Carroll, D. M. and Sleep, B. E., 2007, "Hot Water Flushing for Immiscible Displacement of a Viscous NAPL," *J. Contam. Hydrol.*, Vol. 91(1–4), pp. 247–266.

Ouyang, Y., Cho, J. S., and Mansell, R. S., 2002, "Simulated Formation and Flow of Microemulsions During Surfactant Flushing of Contaminated Soil," *Water Res.*, Vol. 36(1), pp. 33–40.

Pankow, J. F. and Cherry, J. A., 1996, *Dense Chlorinated Solvents and Other NAPLs in Groundwater*, Waterloo Press, Portland.

Rashidi, M., Dehmeshki, J., Daemi, F., Cole, L., and Dickenson, E., 1997, "Color Image Analysis of Contaminants and Bacteria Transport in Porous Media," *Proc. SPIE*, Vol. 3159, pp. 276–286.

Robert, T., Martel, R., Conrad, S. H., Lefebvre, R., and Gabriel, U., 2006, "Visualization of TCE Recovery Mechanisms Using Surfactant-Polymer Solutions in a Two-Dimensional Heterogeneous Sand Model," *J. Contam. Hydrol.*, Vol. 86(1–2), pp. 3–31.

Slavik, J., 1994, *Fluorescent Probes in Cellular and Molecular Biology*, CRC Press, Boca Raton.

Theodoropoulou, M. A., Karoutsos, V., Kaspiris, C., and Tsakiroglou, C. D., 2003, "A New Visualization Technique for the Study of Solute Dispersion in Model Porous Media," *J. Hydrol.*, Vol. 274(1–4), pp. 176–197.

Welker, A., Bowder, J., and Gilbert, R., 1999, "Applied Research Using Transparent Material with Hydraulic Properties Similar to Soil," *Geotech. Test. J.*, Vol. 22(3), pp. 266–270.

Yoon, S., 2006, "Recovery of Coal Tar Using Surfactant Enhanced Aquifer Remediation," Ph.D. dissertation, Polytechnic University, New York.